Early-Onset Lymphoma and Extensive Embryonic Apoptosis in Two Domain-Specific *Fen1* Mice Mutants

Elisabeth Larsen,[1] Liv Kleppa,[1] Trine J. Meza,[3] Leonardo A. Meza-Zepeda,[2,4] Christina Rada,[6] Cesilie G. Castellanos,[1] Guro F. Lien,[1] Gaute J. Nesse,[1] Michael S. Neuberger,[6] Jon K. Laerdahl,[1] Richard William Doughty,[5] and Arne Klungland[1]

[1]Centre for Molecular Biology and Neuroscience and Institute of Medical Microbiology, Rikshospitalet Medical Center and University of Oslo; [2]Norwegian Microarray Consortium, Department for Molecular Biosciences, Faculty of Mathematics and Natural Sciences, and [3]Department of Molecular Biosciences, University of Oslo; [4]Department of Tumor Biology, Institute for Cancer Research, Radiumhospitalet, Rikshospitalet Medical Center; [5]Department of Safety, PCS Biology, GE Healthcare Bio-sciences, Oslo, Norway; and [6]Medical Research Council Laboratory of Molecular Biology, Cambridge, United Kingdom

Abstract

Flap endonuclease 1 (FEN1) processes Okazaki fragments in lagging strand DNA synthesis, and FEN1 is involved in several DNA repair pathways. The interaction of FEN1 with the proliferating cell nuclear antigen (PCNA) processivity factor is central to the function of FEN1 in both DNA replication and repair. Here we present two gene-targeted mice with mutations in FEN1. The first mutant mouse carries a single amino acid point mutation in the active site of the nuclease domain of FEN1 (*Fen1*$^{E160D/E160D}$), and the second mutant mouse contains two amino acid substitutions in the highly conserved PCNA interaction domain of FEN1 (*Fen1*$^{\Delta PCNA/\Delta PCNA}$). *Fen1*$^{E160D/E160D}$ mice develop a considerably elevated incidence of B-cell lymphomas beginning at 6 months of age, particularly in females. By 16 months of age, more than 90% of the *Fen1*$^{E160D/E160D}$ females have tumors, primarily lymphomas. By contrast, *Fen1*$^{\Delta PCNA/\Delta PCNA}$ mouse embryos show extensive apoptosis in the forebrain and vertebrae area and die around stage E9.5 to E11.5. [Cancer Res 2008;68(12):4571–9]

Introduction

The hallmark of most cancers is chromosomal instability, caused by defects in cellular processes (1). Flap endonuclease 1 (FEN1) is associated with many of the processes that help to maintain the integrity of the genome. FEN1 is a multifunctional and structure-specific endonuclease, with roles in DNA repair, replication, and recombination (2). FEN1 recognizes and cleaves single-stranded DNA 5′-flap substrates, which are key intermediates in DNA metabolism. Flap removal by FEN1 is required for the processing of Okazaki fragments (3), long-patch base excision repair (4), and homologous recombination (5). FEN1 interacts with proliferating cell nuclear antigen (PCNA), among other proteins (6). The nuclease activity of FEN1 is greatly improved when bound to PCNA on 5′ flaps and nicked, duplex DNA substrates (5, 7) and the ^{337}QGRLDDFFK^{345} motif is required for this binding (8, 9). Replacing the F343 and F344 residues in FEN1 with glycine and alanine residues, respectively, completely eliminates the physical FEN1-PCNA interaction *in vitro* (10).

The critical role of FEN1 in maintaining genome integrity is shown in studies with *S. cerevisiae*. In these studies, a deletion of *RAD27* (the *S. cerevisiae* homologue of FEN1) exhibits a complex phenotype, including a marked increase in the rate of spontaneous mutations (11). Based on these studies, a FEN1 deficiency is proposed to contribute to several genetic diseases, including cancer and triplet expansion diseases (11, 12). A targeted deletion of the *Fen1* gene in mice causes early embryonic lethality due to proliferation failure (12, 13). Haploinsufficiency of *Fen1* in mice, combined with the adenomatous polyposis coli gene (*Apc*), results in microsatellite instability and can lead to tumor progression (12), thus classifying *Fen1* as a novel tumor suppressor gene (14).

To examine the role of FEN1 in DNA repair and tumorigenesis, we have generated several mouse models with mutations in the *Fen1* gene. We present here two gene-targeted mice carrying site-specific mutations in the *Fen1* gene. The first mutant mouse (*Fen1*$^{E160D/E160D}$) contains a single amino acid mutation in the endonuclease domain of FEN1 (Fig. 1*A* and *C*). The second mutant mouse contains a two-amino-acid point mutation (FEN1 F343G/F344A) in the highly conserved PCNA interaction domain of FEN1 (referred to as *Fen1*$^{\Delta PCNA/\Delta PCNA}$). The rationale for the generation of these two models was based on the biochemical and genetic characterization of mutant enzymes (10, 15–17). The *Fen1*$^{E160D/E160D}$ mice develop a considerably elevated incidence of B-cell lymphomas beginning at 6 months of age, particularly in the females (Fig. 1*B*). *Fen1*$^{\Delta PCNA/\Delta PCNA}$ embryos show extensive apoptosis in the forebrain and vertebrae area and die around stage E9.5 to E11.5.

Materials and Methods

Generation of targeted *Fen1*$^{E160D/E160D}$ and *Fen1*$^{\Delta PCNA/\Delta PCNA}$ mutant mice. See Supplementary Table S1 and Supplementary Figs. S1 to S3.

Morphologic and histologic analyses of mouse embryos. To investigate the stage at which the homozygous *Fen1*$^{\Delta PCNA/\Delta PCNA}$ embryos die, mouse embryos derived from *Fen1*$^{wt/\Delta PCNA}$ × *Fen1*$^{wt/\Delta PCNA}$ crosses were obtained at several stages of gestation, including E8.5, E9.5, E10.5, E11.5, and E12.5. For E9.5, E10.5, and E11.5, at least four litters were collected per stage. All dissections were done in 1× PBS, and the embryo phenotype was studied by light microscopy.

Apoptosis in *Fen1*$^{\Delta PCNA/\Delta PCNA}$ embryos. Deciduas from timed *Fen1*$^{wt/\Delta PCNA}$ heterozygous mating were isolated at E9.5 to E12.5 days postcoitum. Embryos were frozen in Tissue-Tek optimum cutting temperature compound at −80°C and cryosectioned at −10°C (5–10 μm thick). Total and apoptotic nuclei were stained with 4′,6-diamidino-2-phenylindole (DAPI) and the *In Situ* Cell Death Detection Kit, TMR

Note: Supplementary data for this article are available at Cancer Research Online (http://cancerres.aacrjournals.org/).

E. Larsen and L. Kleppa contributed equally to this work.

Requests for reprints: Arne Klungland, Centre for Molecular Biology and Neuroscience and Institute of Medical Microbiology, Rikshospitalet HF and University of Oslo, Sognvannsveien 20, Oslo 0027, Norway. Phone: 47-2307-4072; Fax: 47-2307-4061; E-mail: aklungla@medisin.uio.no.

doi:10.1158/0008-5472.CAN-08-0168

red [terminal deoxyribonucleotidyl transferase–mediated dUTP nick end labeling (TUNEL) staining; Roche], respectively. Five individual knock-in embryos and three individual wild-type embryos were stained two to six times each, with two to three embryo sections on each slide. Stained sections were analyzed with a Zeiss Axioplan 2 microscope and pictures taken with an AxioCamHR.

High- and low-density growth experiments. For the high-density experiments, the *Fen1*$^{E160D/E160D}$ and wild-type mouse embryo fibroblasts (MEF) were plated at 2×10^5 per 6-cm dish. Cells were counted when they reached confluence and replated at 2×10^5 per 6-cm dish. For the low-density experiments, *Fen1*$^{E160D/E160D}$ and wild-type MEFs were plated at a density of 0.5×10^5 per 10-cm dish and their growth rate was monitored by daily counting for 10 d.

Serum starvation and thymidine incorporation. *Fen1*$^{E160D/E160D}$ and wild-type MEF cells were plated in triplicate at 2×10^5 per 3.5-cm dish. After 48 h, the cells were washed twice with PBS and then incubated in DMEM containing 0.1% FCS for 72 h. The cells were fed with DMEM containing 10% FCS. At each time point, the cells were incubated with 5-μCi [^{3}H]thymidine for 1 h at 37°C, washed with PBS, and harvested. [^{3}H]thymidine incorporation was quantified.

FEN1 endonuclease activity on a synthetic DNA flap substrate. Nuclear extracts used for the flap assays were prepared as described previously (18). The flap assay was done with the oligonucleotides sequences provided in Supplementary Table S1, by the method previously described (19).

Histopathology. Full necropsy was done on mice that were found dead after they spontaneously developed disease and mice that were sacrificed due to signs of disease or discomfort. The following tissues were collected and immersion fixed in 10% neutral-buffered formalin: skeletal muscle, skin, mesenteric lymph node, liver, small and large intestines, pancreas, lungs, spleen, kidney, heart, thymus, adrenal gland, pituitary gland, and brain. Any macroscopic abnormalities were noted. After fixation, tissues were trimmed, embedded in paraffin, sectioned at 5 μm, and stained with H&E and Giemsa stain. To evaluate T-cell (CD3) and B-cell (CD45R) populations within the neoplasms, immunohistochemistry was done on sections of the spleen, thymus, mesenteric lymph node, and any macroscopic abnormalities, as previously described. All tissues were examined by a veterinary pathologist using light microscopy. Lymphoid neoplasms were diagnosed using the Bethesda proposals for classification of lymphoid neoplasms in mice (20).

Somatic hypermutation and *in vitro* switching. The somatic hypermutation was done on Peyers patches of 4- to 6-mo-old wild-type and *Fen1*$^{E160D/E160D}$ mice as described previously (21). The efficiency of *in vitro* class switching in wild-type and *Fen1*$^{E160D/E160D}$ spleen B cells was measured as described (22). See Supplementary data for further details.

Comparative genomic hybridization. See Supplementary data.

Mouse FEN1 structural model. A model of mouse FEN1 interacting with PCNA was generated with standard comparative modeling using SWISS-MODEL (23), based on the crystal structure 1UL1 of the human FEN1-PCNA complex from Sakurai and colleagues (24). A model for the active site of the protein including bound water and the two active-site Mg^{2+} ions was generated from the *Methanococcus jannaschii* FEN1 crystal structure 1A77 of Hwang and colleagues (25). The protein structure illustrations were prepared with PyMOL.

Results

Targeting strategy for *Fen1*$^{E160D/E160D}$ and *Fen1*$^{\Delta PCNA/\Delta PCNA}$ mutant mice. To circumvent the embryonic lethality that results from deleting the entire *Fen1* gene, we have generated two alternative *Fen1* mutant mice (Supplementary Table S1; Supplementary Figs. S1–S3). In the first, we mutated a single active-site residue (E160D) in the nuclease core domain of FEN1; in the second, we mutated two residues of FEN1 that are essential for the FEN1-PCNA interaction (F343G/F344A; Fig. 1*A* and *C*). The eight

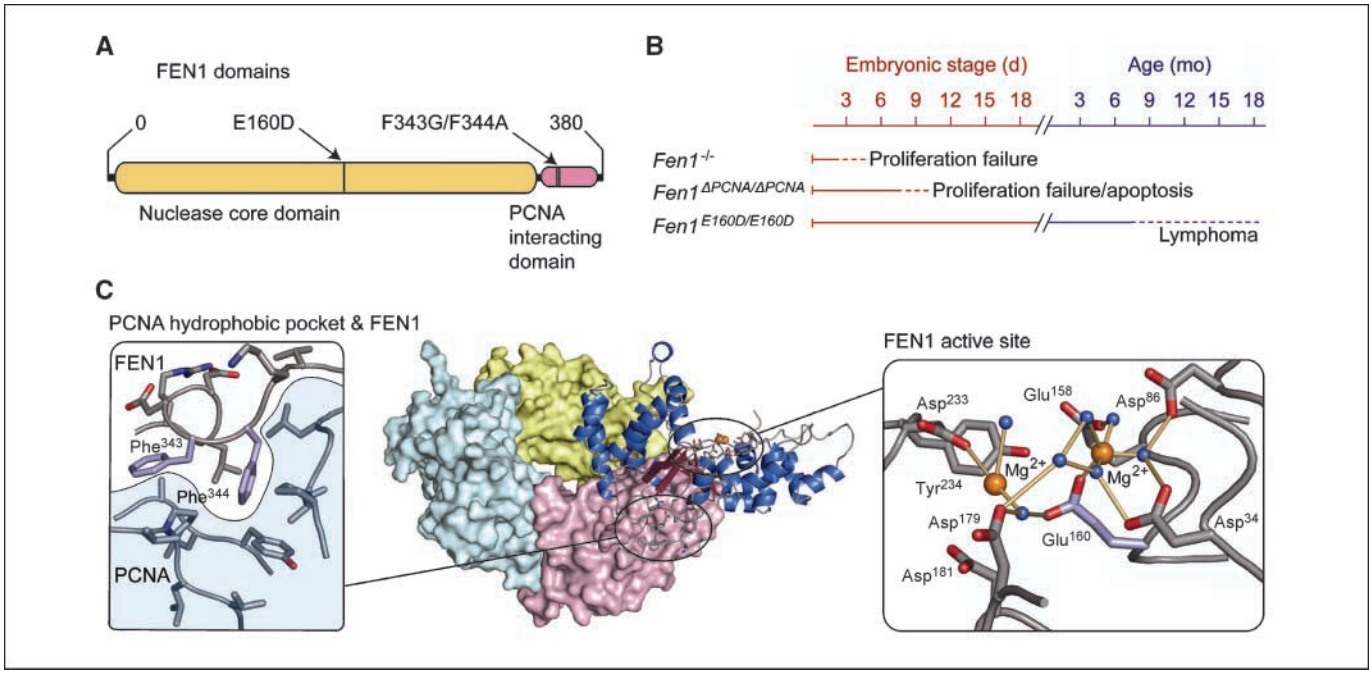

Figure 1. Mouse FEN1 structure and mutations. *A,* site-directed mutations were introduced in the nuclease core domain (residues 1–332) and in the PCNA-interacting COOH-terminal tail (residues 333–380) of FEN1. *B, Fen1* knockout embryos die early around day 4 in embryonic development; *Fen1*$^{\Delta PCNA/\Delta PCNA}$ embryos die around day 10; and *Fen1*$^{\Delta E160D/\Delta E160D}$ mice are phenotypically normal until they develop B-cell lymphoma from 6 mo. *C,* models of mouse FEN1 interacting with PCNA and the FEN1 active site were generated with standard comparative modeling. *Middle,* FEN1 (ribbon rendering) interacts with one of the units of the PCNA homotrimer (surface rendering in pink, cyan, and yellow). *Left,* the FEN1 conserved residues Phe^{343}, Phe^{344}, and Leu^{340} are inserted into a hydrophobic pocket on the PCNA surface (*light blue*) lined by PCNA residues Leu^{126}, Ile^{128}, Pro^{129}, Pro^{234}, Tyr^{250}, and other residues with apolar side chains. *Right,* eight conserved active-site residues bind two Mg^{2+} ions (*orange balls*) and several water molecules (*blue balls*) in a network of hydrogen and coordination bonds.

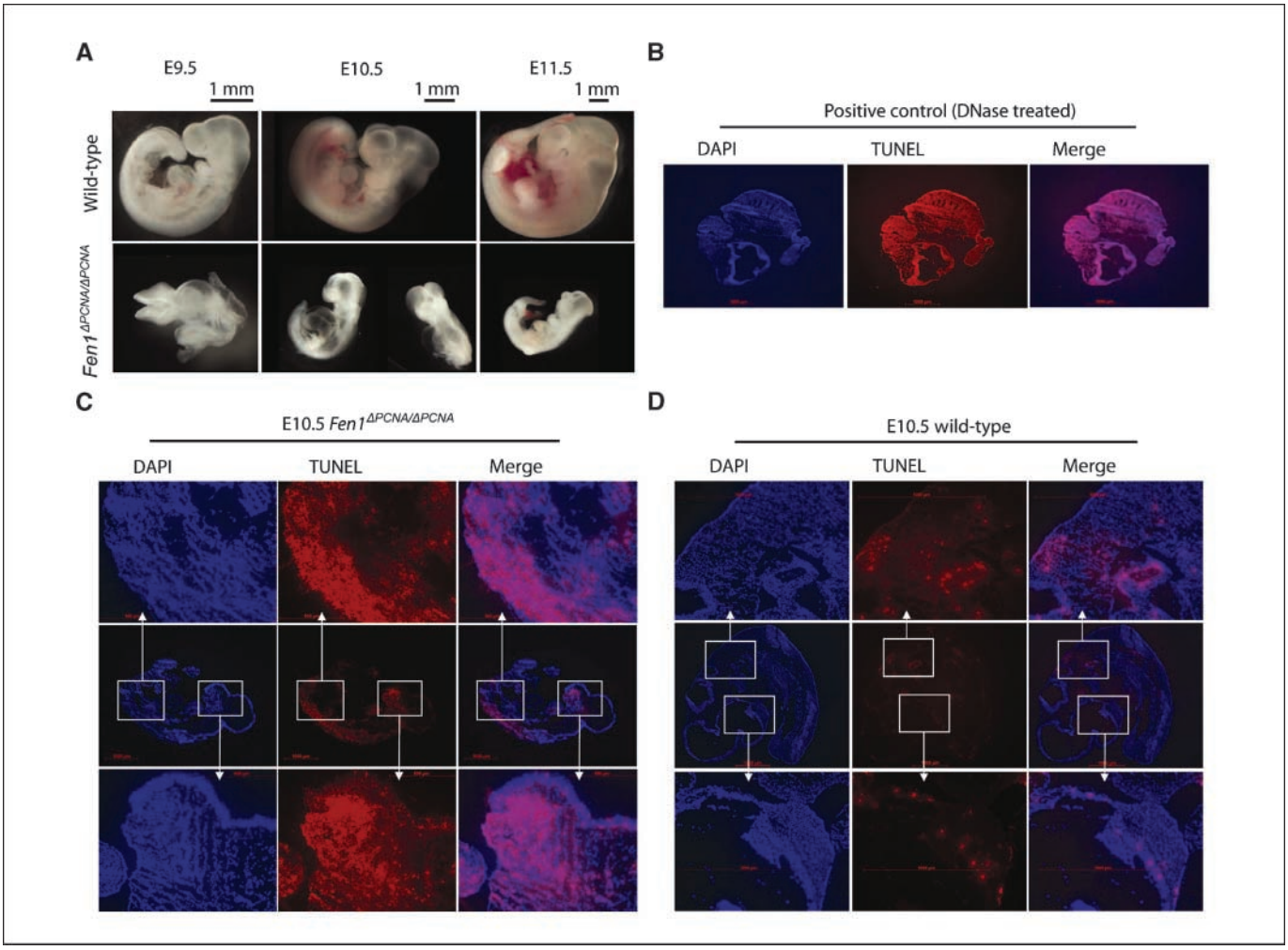

Figure 2. Lethality of $Fen1^{\Delta PCNA/\Delta PCNA}$ embryos. *A,* comparison of $Fen1^{\Delta PCNA/\Delta PCNA}$ (*bottom*) and wild-type (*top*) littermate embryos at stages E9.5, E10.5, and E11.5. $Fen1^{\Delta PCNA/\Delta PCNA}$ embryos are characterized by an open neural fold, pale appearance, the lack of the E8.5 mouse embryo changing its body bending pattern of the abdomen and dorsal parts, from a U-shaped inverted blastoderm to a C-shaped body by E9.5. All $Fen1^{\Delta PCNA/\Delta PCNA}$ embryos were drastically growth retarded at E10.5. However, the heart is relatively big and, in some cases, beating. By E11.5, the $Fen1^{\Delta PCNA/\Delta PCNA}$ embryos are dead, and they are resorbed by E12.5. *B–D,* DAPI (*blue, left* in B–D) and TUNEL (TMR *red, middle* in *B–D*) staining of total and apoptotic nuclei, respectively, on E10.5 embryo cryosection. *Right (B–D)*, DAPI and TUNEL staining is merged. *B,* DNase-treated (3,000 units/mL) cryosectioned wild-type embryos used as a positive control show TUNEL (*red*) staining in virtually all cells. *C,* $Fen1^{\Delta PCNA/\Delta PCNA}$ cryosectioned embryos show extensive apoptosis, especially in the forebrain and along the vertebrae. *D,* wild-type cryosectioned embryos show some apoptosis, which is expected during normal embryonic development. *Middle* (*C* and *D*), *horizontal middle,* whole embryo; sections from the back of the embryo (*top*) and forebrain (*bottom*) are shown at higher magnification. *Bar,* 1000 μm (except *C, top* and *bottom,* 500 μm).

active-site residues of the FEN1 nuclease domain (Fig. 1*C*) are absolutely conserved from archaea to yeast, nematodes, and vertebrates. These active-site residues coordinate at least two divalent cations in a highly conserved geometry. This geometry makes the nuclease domain of FEN1 ideal for binding DNA and the nucleophilic attack of phosphodiester bonds in the DNA-flap backbone. The E160D mutation has previously been shown to reduce the *in vitro* endonuclease activity of FEN1 to around 10% to 20%, relative to the wild-type enzyme, whereas the PCNA interaction domain remains intact and functional (15). The two mutated phenylalanines in FEN1 [i.e., the conserved residues F343 and F344 of the classic PCNA-interacting protein motif (PIP-box); ref. 8] are absolutely required for the PCNA interaction (10). These phenylalanines in FEN1 are inserted into a hydrophobic pocket on the surface of PCNA (Fig. 1*C*). The details of the site-directed mutagenesis and gene targeting are included in full in Supplementary data. The targeted *Fen1* loci were expressed at wild-type levels, and the targeting did not affect the expression of other genes approximate to the targeted *Fen1* gene (Supplementary Table S2; Supplementary Fig. S4).

The PCNA interaction domain of FEN1 is critical for full neonatal viability. Interbreeding of heterozygous mice carrying the FEN1 F343G/F344A residues failed to produce homozygous $Fen1^{\Delta PCNA/\Delta PCNA}$ mice. We observed that at E10.5, all $Fen1^{\Delta PCNA/\Delta PCNA}$ embryos were drastically growth retarded, showing significantly reduced overall size and defective development as compared with their littermates (Fig. 2*A*). They were characterized by an open neural fold, pale appearance, the lack of the E8.5 mouse embryo changing its body bending pattern of the abdomen and dorsal parts, from a U-shaped inverted blastoderm to a C-shaped body by stage E9.5, and a high degree of apoptosis (Fig. 2). At E11.5 to E12.5, only dead or massively growth-retarded $Fen1^{\Delta PCNA/\Delta PCNA}$ embryos were evident, with most already in the

process of resorption (Supplementary Table S3). Attempts to establish MEF cell lines from E10.5 *Fen1*$^{\Delta PCNA/\Delta PCNA}$ failed, despite several attempts. In parallel experiments, cell lines were routinely established from the wild-type and heterozygous littermates. No living *Fen1*$^{\Delta PCNA/\Delta PCNA}$ embryos were found at or after stage E12.5, when a total of 193 embryos from heterozygous matings were analyzed (Supplementary Table S3). Mice heterozygous for the F343G/F344A mutation were fertile and phenotypically indistinguishable from wild-type mice.

E160D cells have a proliferation defect under low-density culture conditions. In contrast to the embryonic lethal phenotype observed in the *Fen1*-null mice, interbreeding of *Fen1*$^{wt/E160D}$ led to the recovery of the expected genotypes with Mendelian ratios (data not shown). A DNA 5′-flap endonuclease assay confirmed that the activity of the FEN1 E160D protein is reduced to ~20% compared with the wild-type enzyme (ref. 17; Fig. 3*A*), in good agreement with the *in vitro* biochemical assays. MEF cells from wild-type and *Fen1*$^{E160D/E160D}$ littermates were cultured under high- or low-density conditions to determine if the E160D mutation affected the rate of cellular proliferation. At high cell density, the growth rate of *Fen1*$^{E160D/E160D}$ cells was comparable to, but lower than, the wild-type control cells. The cellular duplication rate was ~12 hours for wild-type MEF cells and 17 hours for the *Fen1*$^{E160D/E160D}$ MEF cells (data not shown). The proliferation defect of the *Fen1*$^{E160D/E160D}$ cells became considerably more apparent under low-density culture conditions (Fig. 3*B, left*). The extent of apoptosis observed in the wild-type MEFs was similar to the level of apoptosis in the *Fen1*$^{E160D/E160D}$ MEFs. These results suggest that the proliferation defect observed in the *Fen1*$^{E160D/E160D}$ MEF cells is due to a defect in cell division rather than the induction of apoptosis or premature senescence. These results also support the hypothesis that the endonuclease activity of FEN1 is essential during Okazaki fragment maturation.

***Fen1*$^{E160D/E160D}$ MEF cells have a cell cycle defect.** To understand the nature of the *Fen1*$^{E160D/E160D}$ proliferation defect, we compared the cell cycle progression of wild-type MEFs to that

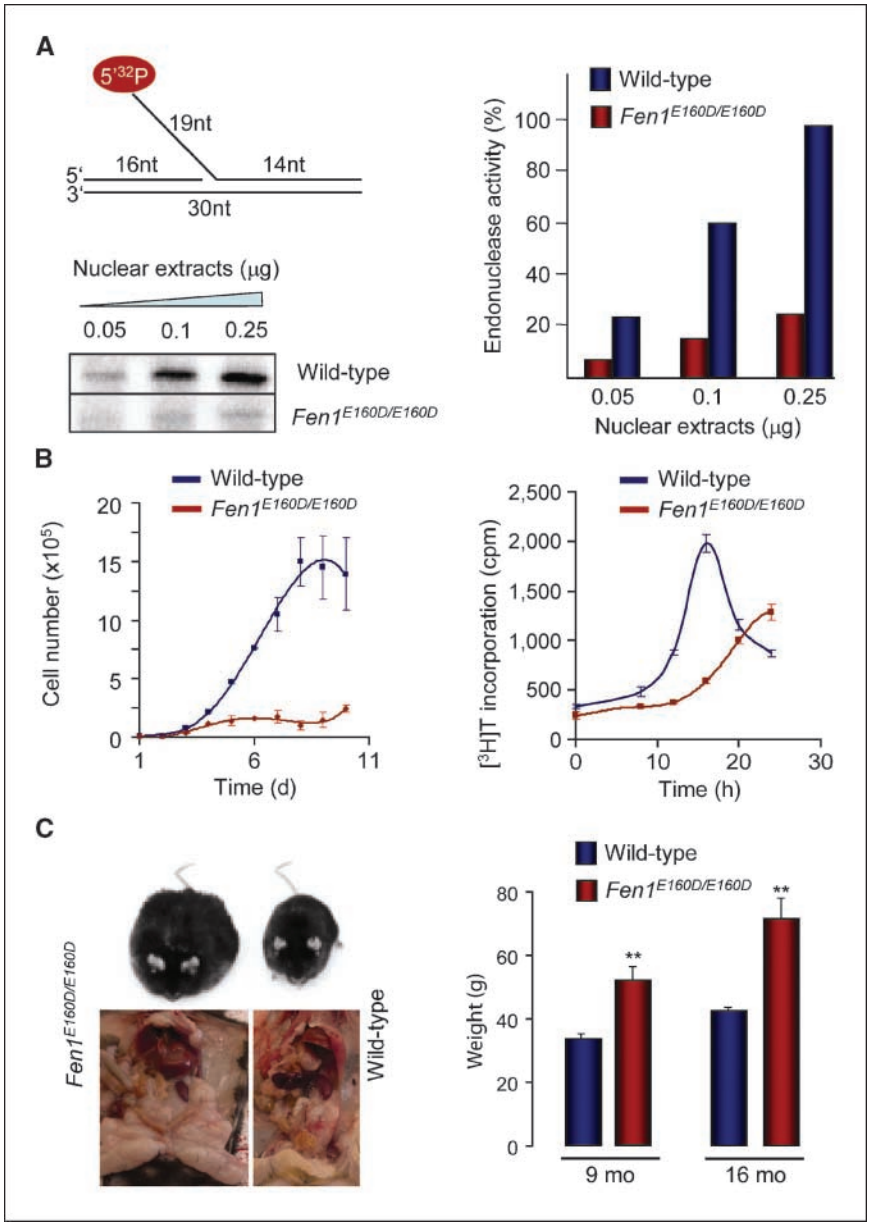

Figure 3. Characterization of the *Fen1*$^{E160D/E160D}$ mice. *A, left,* structure and cutting of DNA flap substrate. Nuclear extracts from MEFs were prepared as described (Materials and Methods). *Right,* quantification of endonuclease activity for wild-type and *Fen1*$^{E160D/E160D}$ mice. *B, left,* proliferation of wild-type and *Fen1*$^{E160D/E160D}$ MEFs under low-density conditions. *Right,* cell cycle progression of wild-type and *Fen1*$^{E160D/E160D}$ MEFs by [^{3}H]thymidine incorporation. *C, left,* images of *Fen1*$^{E160D/E160D}$ mice. It depicts the age-matched comparison of a morbidly obese knock-in female with a wild-type female at ~10 mo of age. Necropsies revealed extensive fat deposits in the subcutis, retroperitoneum, abdomen, and mediastinum. *Right,* body weight of wild-type and *Fen1*$^{E160D/E160D}$ mice at 9 mo (9 *Fen1*$^{E160D/E160D}$ mice and 16 wild-type mice) and 17 mo (4 *Fen1*$^{E160D/E160D}$ mice and 4 wild-type mice). **, $P \leq 0.001$.

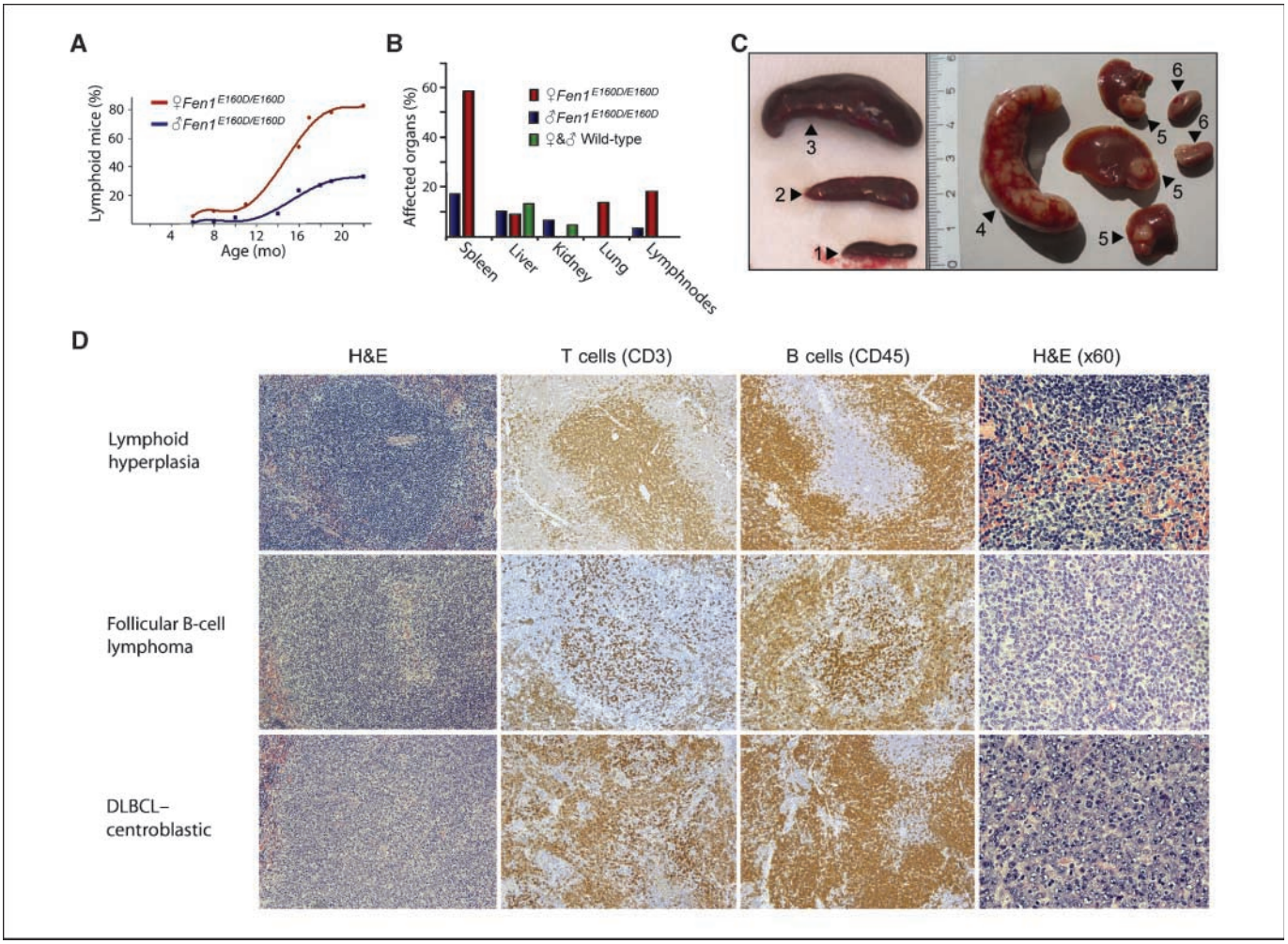

Figure 4. The *Fen1*$^{E160D/E160D}$ mice develop B-cell lymphoma. *A,* tumor incidence in *Fen1*$^{E160D/E160D}$ mice. The percentage of lymphoid *Fen1*$^{E160D/E160D}$ mice is plotted against time (in months). *B,* affected organs. Wild-type control mice are included to show that no lymphoma was identified in the control group. *C,* macroscopic appearance of a normal spleen (*1*), a spleen with lymphoid hyperplasia (*2*), and a spleen with follicular B-cell lymphoma (*3*). The animals with lymphoma commonly had tissue involvement other than the spleen (4) including the mesenteric lymph node, which is often diffusely enlarged (not shown), liver (*5*), which typically had white variably sized focal nodules randomly distributed throughout the parenchyma (*arrows*), and kidney (*6*), which was typically diffusely enlarged and pale. *D,* histologic studies of the spleen from *Fen1*$^{E160D/E160D}$ mice. *Top,* lymphoid hyperplasia. The follicles are enlarged, and the marginal zone, PALS, and the red pulp seem to be normal. The T cells (CD3) are concentrated in the PALS with smaller numbers present in the red pulp, and the B cells (CD45R) are surrounding the PALS. *Middle,* follicular B-cell lymphoma. The pale zone surrounding the arteriole represents the loss of the PALS and replacement with mixed centroblasts and centrocytes. Both T cells (CD3) and B cells (CD45R) are present throughout the follicular structure. The lymphoma consists of mixed cell populations (H&E, ×60). *Bottom,* DLBCL of the centroblastic subtype (*DLBCL-CB*). Note the diffuse involvement of the entire spleen and the effacement of the normal splenic structure. Throughout the spleen, T cells (CD3) and B cells (CD45R) are admixed and do not form any structures. The neoplasm consists of a uniform population of large centroblasts with characteristic nucleoli that adhere to the nuclear membrane. Magnification, ×40 (unless indicated otherwise).

of *Fen1*$^{E160D/E160D}$ MEFs. The cells were serum starved for 72 hours before serum addition giving a coordinated reentry into the cell cycle. After the addition of serum, the MEFs were harvested at regular intervals and labeled with [^{3}H]thymidine for 1 hour to monitor DNA synthesis (Fig. 3*B, right*). The wild-type MEFs began incorporating [^{3}H]thymidine 8 to 12 hours after serum stimulation and showed maximal levels of [^{3}H]thymidine incorporation at 16 to 20 hours. In contrast, the *Fen1*$^{E160D/E160D}$ MEFs showed significantly reduced levels and a reduced rate of [^{3}H]thymidine incorporation.

***Fen1*$^{E160D/E160D}$ mice develop obesity in the absence of insulin resistance or diabetes.** Within the first generation, approximately half of the *Fen1*$^{E160D/E160D}$ mice, both males and females, developed marked obesity by 9 months of age, compared with the age-matched wild-type controls (*Fen1*$^{E160D/E160D}$, 48 ± 3 g; wild-type control, 31 ± 1 g; $P < 0.001$; Fig. 3*C*). This difference in body weight was even greater at 16 months (*Fen1*$^{E160D/E160D}$, 65 ± 5 g; wild-type control, 39 ± 1 g; $P \leq 0.001$). *Fen1*$^{E160D/E160D}$ and wild-type control mice were raised under identical conditions and fed standard rodent chow.

A marked increase in the amount of white adipose tissue was seen in the subcutis, retroperitoneum, abdomen, mediastinum, and around the epididymes on necropsy (Fig. 3*C, left*). All other organs examined, including the interscapular brown adipose tissue, seemed of similar size to those of control mice. Histologic examination of adipose tissues revealed a minimal/mild hypertrophy of the white adipose cells and no changes in the brown adipose tissue. Analysis of the glucose, insulin, and leptin levels revealed the obese *Fen1*$^{E160D/E160D}$ mice to be normoglycemic, normoinsulinemic, and normoleptinemic (data not given), indicating that the

observed obesity was not associated with an insulin resistance or type 2 diabetes mellitus. Supporting this hypothesis, we noted no histologic changes in the size of the pancreatic islets in the *Fen1*$^{E160D/E160D}$ mice compared with age-matched, wild-type controls.

Female *Fen1*$^{E160D/E160D}$ mice develop lymphoid hyperplasia and lymphoma with multiorgan involvement. Macroscopic evaluations of the *Fen1*$^{E160D/E160D}$ mice revealed that most of the female mice (Fig. 4*A*) had developed a diffuse enlargement of the spleen, which, when cross-sectioned, showed multifocal to coalescing white areas (Fig. 4; Table 1). The lung (97% of cases), liver (93%), kidneys (90%), mesenteric lymph nodes (62%), and thymus (55%) commonly showed enlargement or focal changes in association with the splenic enlargement (Fig. 4*B* and *C*). The lung, liver, and kidneys contained multifocal, white nodular foci randomly distributed through the organs, whereas mesenteric lymph nodes and thymus were often diffusely enlarged. Microscopic evaluation of the spleens showed lymphoid hyperplasia, follicular lymphoma, and diffuse large B-cell lymphoma (DLBCL) of the centroblastic type (Fig. 4*D*). One mouse was diagnosed with a histiocytic sarcoma.

The lymphoid hyperplasia showed normal splenic architecture, although the follicles were enlarged and more numerous. The marginal zone was often expanded with the periarteriolar sheaths (PALS) appearing to be normal. No abnormalities were detected in the red pulp. The CD3-positive cells (T cells) were concentrated around the PALS and were comparable in size and number with the wild-type controls. The CD45R-positive cells (B cells) were increased in number and were concentrated around the PALS, within the marginal zone, and scattered within the red pulp. Follicular B-cell lymphomas showed the uniform enlargement and coalescence of the follicles of white pulp, and a loss of the distinct marginal zones and PALS was not observed. The white pulp contained a mixed cell population with cytologic features similar to centroblasts and centrocytes. CD45R and CD3 staining showed B cells and T cells, respectively, throughout the altered follicular structure. The red pulp was compressed or reduced. The DLBCL of the centroblastic type consisted of diffuse involvement of the spleen and the effacement of the splenic architecture. Within the white pulp, the majority of the cells were of the centroblastic type, being of medium size and containing little cytoplasm, round vesicular nuclei, and prominent nucleoli. The CD45R and CD3 immunostaining showed B cells and T cells intermingled throughout the spleen.

Metastases were noted within the lungs, liver, and kidneys. These consisted of multifocal infiltrations of CD45R-positive B cells, often admixed with smaller numbers of CD3-positive T cells. The infiltration of CD45R-positive B cells was often located around blood vessels and often compressed, effacing the normal architecture of the organ. When all the lymphoproliferative lesions (lymphoid hyperplasia, DLBCL of the centroblastic type, and follicular lymphoma) were grouped, the *Fen1*$^{E160D/E160D}$ mice showed a significant increase (both males and females) in these lesions, compared with the wild-type controls ($P < 0.05$). Pulmonary proliferative lesions (epithelial hyperplasia, adenoma, and adenomcarcinoma) were noted in female *Fen1*$^{E160D/E160D}$ mice although the incidence of these lesions, when grouped together, was not statistically higher than in the wild-type controls.

To investigate the extent of the genomic instability of the tumors in *Fen1*$^{E160D/E160D}$ mice, high-resolution array-based comparative genomic hybridization was done using an Agilent 44k oligonucleotide microarray (Supplementary Fig. S5). Fifteen tumors from nine different mice were analyzed against their corresponding controls. Complex genomic rearrangement, involving multiple chromosomes, was observed in three tumors (Supplementary Fig. S5*A–D*). In addition, moderate rearrangements of chromosome or chromosome arms were seen in three samples, as well as tumors with nearly a normal DNA copy number. In total, >50% of the tumors showed aberrations in DNA copy number. Two minimal recurrent regions of alterations were identified in >20% of the tumors (individual animals; Supplementary Fig. S5*E–H*). Loss of 8C3 ($\sim$0.9 Mb) was found in 4 of 9 tumors, and gain of 8C4 ($\sim$0.7 Mb) was identified in 5 of 9 (Supplementary Fig. S4). According to Ensembl (NCBI m37, April 2007), these regions contained 7 and 29 genes, respectively (Supplementary Table S4). No aberrations were observed in the *APC* locus previously found to be linked to tumor formation in *Fen1* mutant mice (12).

Table 1. Proliferative lesions in *Fen1*$^{E160D/E160D}$ mice

Body system	Lesion	No. of cases					% Involvement of organs other than primary tumor site
		Female	% of female	Male	% of male	Total	
Hematopoietic (spleen)	DLBCL (centroblastic)	13	48	3	8	16	100
	Follicular B-cell lymphoma	8	30	7	19	15	100
	Lymphoid hyperplasia, white pulp, spleen	2	7	7	19	9	NA
	Histiocytic sarcoma	1	4	0	0	1	100
Pulmonary	Adenoma, solid	2	7	0	0	2	0
	Adenocarcinoma, solid	1	4	0	0	1	0
	Epithelial hyperplasia	3	11	0	0	3	NA
Mammary gland	Fibroadenoma	1	4	0	0	1	0
	No abnormality detected	2	7	16	44	18	NA
	No. mice evaluated	27		36		63	NA

Abbreviation: NA, not applicable (hyperplasias do not spread).

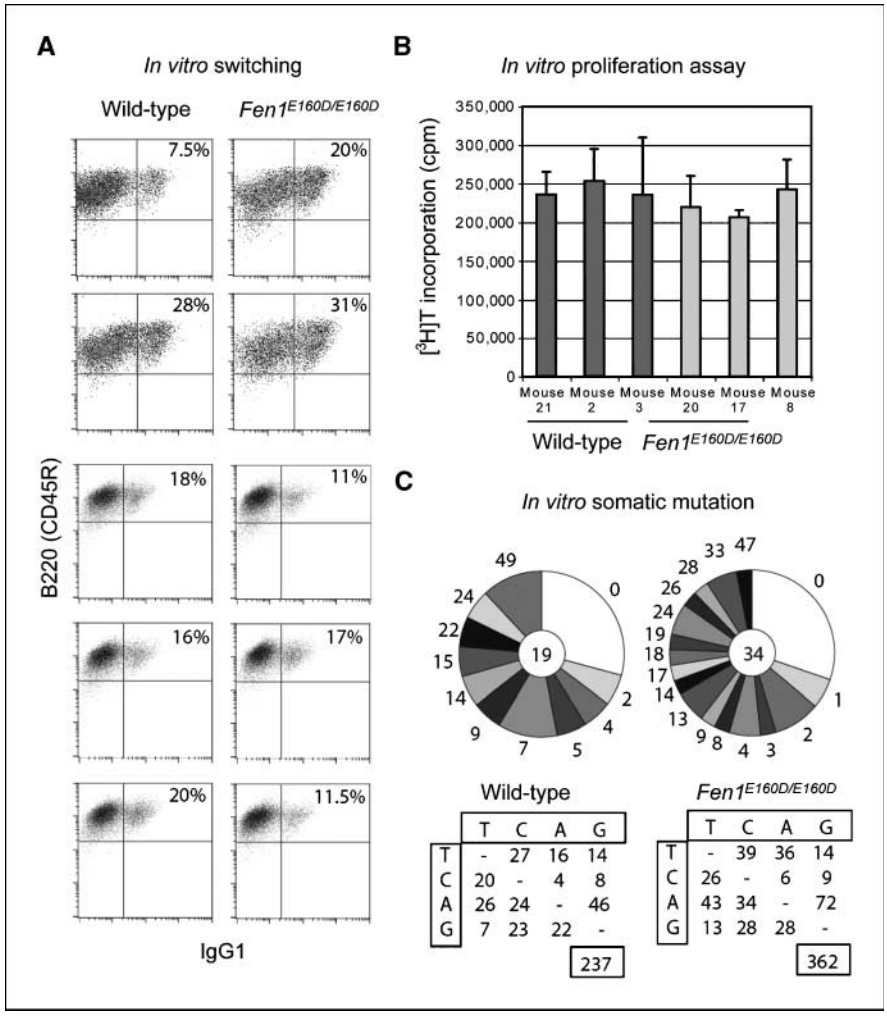

Figure 5. *In vitro* switching and somatic hypermutation in *Fen1*$^{E160D/E160D}$ mice. *A, in vitro* class switching of splenic B cells from wild-type and *Fen1*$^{E160D/E160D}$ mice analyzed by flow cytometry after a 7-d culture in the presence of LPS and IL-4. The percentage of B cells [CD45R(B220) positive] expressing surface IgG1 in each switch culture is shown on the top right-hand corner of the dot plot. The results represent five control mice and five *Fen1*$^{E160D/E160D}$ mice in two separate experiments. *B,* stimulation of B cells from *Fen1*$^{E160D/E160D}$ and wild-type controls showed no appreciable difference in proliferation as measured by [^{3}H]thymidine incorporation. *C,* somatic hypermutation was analyzed by monitoring mutation accumulation in the intronic V_HJ558/J_H rearrangement-flanking region. Pie slices represent the number of clones with the specified number of mutations per clone. The number of sequences analyzed is shown in the central circle. Only nonclonal sequences were included in the analysis by virtue of their unique CDR3 region. In the table, the number of mutations from each nucleotide is shown. The total number of mutations is shown boxed for each database. Data were pooled from two control littermates and two *Fen1* mutant (*Fen1*$^{E160D/E160D}$) mice.

Normal somatic hypermutation and class-switch recombination of immunoglobulin genes in *Fen1*$^{E160D/E160D}$ mice. Defects in class-switch recombination and somatic hypermutation are processes in the B cells, which are often associated with B-cell lymphoma. To examine the effects of reduced FEN1 activity on class-switch recombination, we stimulated B cells purified from spleens of native 4- to 6-month-old littermates of wild-type and *Fen1*$^{E160D/E160D}$ mice, using lipopolysaccharide (LPS) or LPS and interleukin-4 (IL-4), which will induce class-switch recombination (Fig. 5). LPS stimulation *in vitro* in the presence of IL-4 induces B cells to undergo class-switch recombination from IgM to IgG1 (26). Cells were cultured for 4 days and analyzed by flow cytometry for surface expression of the expected isotopes (Fig. 5*A*). These *in vitro* data showed that class-switch recombination seemed to be normal in the *Fen1*$^{E160D/E160D}$ mice. Additionally, stimulated B cells from *Fen1*$^{E160D/E160D}$ and wild-type controls showed no appreciable difference in proliferation, as measured by [^{3}H]thymidine incorporation (Fig. 5*B*), indicating that reduced FEN1 activity did not result in an obvious defect in B-cell proliferation.

We also analyzed somatic hypermutation in the mutant mice by monitoring mutation accumulation in the intronic V_HJ558/J_H rearrangement-flanking region. This intronic region was PCR amplified from germinal center B cells from Peyer's patches of 5- to 7-month-old mice, and sorted by virtue of their PNA^{hi} CD45R(B220)$^+$ phenotype. No divergence was found from the pattern in control animals (Fig. 5*C*).

Discussion

Elucidating the molecular events that occur at the onset of B-cell lymphomas is essential for several reasons. Diffuse large cell lymphoma is an aggressive B-cell malignancy that accounts for 40% of non-Hodgkin's lymphomas and is the most common type of lymphoma in adults (27). Due to its heterogeneous presentation, diffuse large cell lymphoma gives rise to significant individual-level differences in responsiveness to therapy and a 60% mortality, making treatment decisions difficult (28). We show in this study the results of two *Fen1* knock-in mice, which show that a decrease in FEN1 activity causes abnormal cell proliferation, genomic instability, and tumorigenesis.

The currently understood role of FEN1 at critical DNA structures generated as base excision repair intermediates possibly explains the tumor phenotype of *Fen1*$^{E160D/E160D}$ mice. In mammalian cells, 20,000 to 50,000 DNA-damaging events occur per day; some of these DNA damage events include single-strand breaks, depurination of DNA bases, and oxidation of DNA bases. The base excision repair pathway repairs most of the damages associated with this spontaneous decay of the DNA helix (29).

Several base excision repair–deficient mice have been generated, but the majority of these mice are not associated with a cancer-prone phenotype (30). Two exceptions are the cancer-prone *Ogg1/MutY* double mutant mice and UNG-deficient mice (22, 31). A UNG deficiency in mice causes a lymphoproliferative disorder with lymphoid hyperplasia and a 22-fold increase in the risk of developing B-cell lymphoma, a phenotype similar to that of a $Fen1^{E160D/E160D}$ knock-in mouse. Lymphoma development in UNG-deficient mice is explained by reduced class-switch recombination and skewed somatic hypermutation (22). Loss of regulation of somatic hypermutation is observed in >50% of DLBCLs (32). Despite a similar phenotype, these processes do not seem to be affected in $Fen1^{E160D/E160D}$ mice. Cell lines derived from $Fen1^{E160D/E160D}$ mutant mice show that the E160D mutation reduces the rate of cellular proliferation in MEF cells. This observation is consistent with the role of FEN1 in removing the RNA primer during DNA replication and several studies conclude that lymphomagenesis involves changes in the expression of genes that are important for proliferation (33).

$Fen1^{E160D/E160D}$ mice develop a 20-fold increased incidence of early onset hematopoietic malignancy, principally attributable to DLBCL and follicular B-cell lymphoma, and females develop lymphomas at a higher incidence than males. This skewed tumor ratio between the sexes is also seen by others (34). The reason for the gender differences observed in mouse lymphoma is not well understood. One can speculate that sex hormones, such as estrogen, could result in the observed skewed tumor ratio between the sexes. The sex hormones are involved in both normal development and immunomodulating processes of the cell (e.g., estrogen influences immunoglobulin levels in postpubertal female mice and is involved in the adaptive immune system). In a recent study, FEN1 was suggested to modulate the estrogen-responsive gene expression (35).

The finding that female $Fen1^{E160D/E160D}$ mice have an increased incidence of proliferative pulmonary lesions must be evaluated with caution. It has been documented that the 129 strain mice can have a high incidence (up to 40%) of spontaneous lung tumors (36). Although backcrossing is done to remove extraneous genetic material, the 129 strain may still have an influence on the phenotypic lesion observed (37). Therefore, the different genetic background of two $Fen1^{E160D/E160D}$ knock-in studies could explain the intriguing difference in the tumor phenotypes (38). Yet, both studies conclude that genomic instability caused by inadequate FEN1 activity leads to a considerably elevated spontaneous tumor incidence. In the study by Zheng and colleagues (38), several mutations affecting the nuclease activity of FEN1 were identified in human cancer specimens. The remarkable different tumor manifestation could imply that in a heterogeneous population, represented in the studies described above by two different inbred mouse strains, mutations or single-nucleotide polymorphisms in other genes might be important for the tumor type. Large-scale evaluations of common genetic variants in the human population support this notion. One such study evaluated the association between single-nucleotide polymorphisms in DNA repair genes and risk of non-Hodgkin's lymphoma in a population-based case-control study. Single-nucleotide polymorphisms in DNA repair genes were associated with altered risk of non-Hodgkin's lymphoma and DLBCL, the major B-cell subtype (39).

The detrimental phenotype found in our $Fen1^{\Delta PCNA/\Delta PCNA}$ embryos is far more severe than the phenotype observed in another related study (40). In our $Fen1^{\Delta PCNA/\Delta PCNA}$ embryos, we identified an embryonic lethal phenotype at E9.5 to E10.5; however, Zheng and colleagues reported a phenotype with newborn lethality. Additionally, they reported replication defects, pulmonary hypoplasia, and pancytopenia. Our $Fen1^{\Delta PCNA/\Delta PCNA}$ embryos showed defective organogenesis, which could explain the significant defects in the growth and the development of the lung and the blood system (40). The noticeable difference between these two FEN1 ΔPCNA models could be explained by different amino acid mutations. In one study, the two phenylalanines, in the conserved PIP box of FEN1 (41), were mutated to alanines (FF to AA), whereas in the other study, the two phenylalanines were replaced with glycine and alanine (FF to GA; 343, 344). Glycine can cause increased peptide backbone flexibility compared with alanine because it is lacking the small aliphatic side chain. Gomes and Burgers (10) previously characterized the FF to GA mutant of the conserved PCNA interacting domain in yeast FEN1. With this mutant of FEN1, they observed a severely decreased interaction with PCNA, which resulted in replication and repair defects *in vivo*. An FF to AA mutant in the PIP box domain of the CDC9 DNA ligase had a less severe effect, when compared with the FEN1 FF to GA mutation, on the CDC9-PCNA interaction (42). Our $Fen1^{\Delta PCNA/\Delta PCNA}$ embryos did not properly undergo gastrulation (start at stage E6), neurulation, cardiogenesis, somitogenesis, or body folding (all events start at E7–E7.5), and the defective embryonic development ended in apoptosis and death around midgestation. Embryo stages E6 to E12.5 show rapid cell proliferation in the normal developing embryo. The detrimental phenotype observed in embryos leads us to conclude that the FEN1 interaction with PCNA is crucial for rapidly proliferating cells in the mouse embryo. On the other hand, if FEN1 cannot interact with PCNA, it must be recruited to the replication machinery by other mechanisms to avoid very early embryonic lethality. To date, at least 20 proteins are reported to interact with FEN1. Each of the known interacting proteins can be categorized based on the role in which they assist FEN1 in DNA repair, replication, apoptosis, or cell cycle control (2). During DNA lagging strand replication, in addition to PCNA, FEN1 interacts with DNA polymerase δ, replication protein A, and DNA ligase I, in addition to Werner and Bloom proteins (6). Similar to PCNA, Bloom and Werner proteins can stimulate FEN1 activity *in vitro* (43). FEN1 also interacts with chromatin to accomplish its role in DNA replication (41). Thus, FEN1 might get access to flap substrates during replication through binding to a core histone tail. Some of these interactions might enable mutated FEN1 to perform limited nuclease activity at the replication fork without interacting with PCNA.

We observed marked obesity by 9 months of age in male and female $Fen1^{E160D/E160D}$ mice. In the last year, several exciting studies have observed obesity and severe metabolic defects in mice carrying specific defects in base excision repair (44, 45). Moreover, the obesity-associated *FTO* gene was recently shown to encode a 2-oxoglutarate–dependent nucleic acid demethylase (46). It is now important to determine whether altered DNA repair activities underlie altered food intake or energy expenditure, or both. A systematic review recently identified a link between increased body mass index and increased risk of common and less common malignancies, and for some cancer types association differs between sexes and populations of different ethnic origins (47). Such data also support the notion above about the different tumor types observed in two different mouse strains carrying the $Fen1^{E160D}$ alleles.

In conclusion, we report here of two different *Fen1* mutant mice with a dramatic difference between the nuclease-defective mouse and the strain defective in PCNA binding, showing that the interaction with PCNA is extremely important to ensure FEN1 being accurately recruited to DNA 5′-flap substrates, which are key intermediates in DNA metabolism.

Disclosure of Potential Conflicts of Interest

No potential conflicts of interest were disclosed.

Acknowledgments

Received 1/15/2008; revised 3/10/2008; accepted 3/26/2008.

Grant support: National Program in Functional Genomics sponsored by the Norwegian Research Council, the Norwegian Cancer Society, and the University of Oslo (EMBiO). This work was supported by the National Microarray platform of the Functional Genomics program of the Research Council of Norway.

The costs of publication of this article were defrayed in part by the payment of page charges. This article must therefore be hereby marked *advertisement* in accordance with 18 U.S.C. Section 1734 solely to indicate this fact.

We thank Adam Robertson for helpful comments and corrections and the Norwegian Transgenic Center (NTS) and the Center for Comparative Studies at Rikshospitalet Medical Center for excellent service.

References

1. Lengauer C, Kinzler KW, Vogelstein B. Genetic instabilities in human cancers. Nature 1998;396:643–9.
2. Liu Y, Kao HI, Bambara RA. Flap endonuclease 1: a central component of DNA metabolism. Annu Rev Biochem 2004;73:589–615.
3. Rumbaugh JA, Henricksen LA, DeMott MS, Bambara RA. Cleavage of substrates with mismatched nucleotides by Flap endonuclease-1. Implications for mammalian Okazaki fragment processing. J Biol Chem 1999;274:14602–8.
4. Klungland A, Lindahl T. Second pathway for completion of human DNA base excision-repair: reconstitution with purified proteins and requirement for DNase IV (FEN1). EMBO J 1997;16:3341–8.
5. Wu XT, Li J, Li XY, Hsieh CL, Burgers PMJ, Lieber MR. Processing of branched DNA intermediates by a complex of human FEN-1 and PCNA. Nucleic Acids Res 1996;24:2036–43.
6. Shen B, Singh P, Liu R, et al. Multiple but dissectible functions of FEN-1 nucleases in nucleic acid processing, genome stability and diseases. BioEssays 2005;27:717–29.
7. Li X, Li J, Harrington J, Lieber MR, Burgers PM. Lagging strand DNA synthesis at the eukaryotic replication fork involves binding and stimulation of FEN-1 by proliferating cell nuclear antigen. J Biol Chem 1995;270:22109–12.
8. Warbrick E. The puzzle of PCNA's many partners. Bioessays 2000;22:997–1006.
9. Gary R, Ludwig DL, Cornelius HL, MacInnes MA, Park MS. The DNA repair endonuclease XPG binds to proliferating cell nuclear antigen (PCNA) and shares sequence elements with the PCNA-binding regions of FEN-1 and cyclin-dependent kinase inhibitor p21. J Biol Chem 1997;272:24522–9.
10. Gomes XV, Burgers PM. Two modes of FEN1 binding to PCNA regulated by DNA. EMBO J 2000;19:3811–21.
11. Freudenreich CH, Kantrow SM, Zakian VA. Expansion and length-dependent fragility of CTG repeats in yeast. Science 1998;279:853–6.
12. Kucherlapati M, Yan K, Kuraguchi M, et al. Haploinsufficiency of Flap endonuclease (Fen1) leads to rapid tumor progression. Proc Natl Acad Sci U S A 2002;99:9924–9.
13. Larsen E, Gran C, Saether BE, Seeberg E, Klungland A. Proliferation failure and gamma radiation sensitivity of Fen1 null mutant mice at the blastocyst stage. Mol Cell Biol 2003;23:5346–53.
14. Fodde R, Smits R. Cancer biology. A matter of dosage. Science 2002;298:761–3.
15. Frank G, Qiu J, Somsouk M, et al. Partial functional deficiency of E160D flap endonuclease-1 mutant *in vitro* and *in vivo* is due to defective cleavage of DNA substrates. J Biol Chem 1998;273:33064–72.
16. Shen B, Nolan JP, Sklar LA, Park MS. Essential amino acids for substrate binding and catalysis of human flap endonuclease 1. J Biol Chem 1996;271:9173–6.
17. Frank G, Qiu J, Zheng L, Shen B. Stimulation of eukaryotic flap endonuclease-1 activities by proliferating cell nuclear antigen (PCNA) is independent of its *in vitro* interaction via a consensus PCNA binding region. J Biol Chem 2001;276:36295–302.
18. Ringvoll J, Nordstrand LM, Vagbo CB, et al. Repair deficient mice reveal mABH2 as the primary oxidative demethylase for repairing 1meA and 3meC lesions in DNA. EMBO J 2006;25:2189–98.
19. Spiro C, McMurray CT. Nuclease-deficient FEN-1 blocks rad51/BRCA1-mediated repair and causes trinucleotide repeat instability. Mol Cell Biol 2003;23:6063–74.
20. Morse HC III, Kearney JF, Isaacson PG, Carroll M, Fredrickson TN, Jaffe ES. Cells of the marginal zone—origins, function and neoplasia. Leuk Res 2001;25:169–78.
21. Jolly CJ, Klix N, Neuberger MS. Rapid methods for the analysis of immunoglobulin gene hypermutation: application to transgenic and gene targeted mice. Nucleic Acids Res 1997;25:1913–9.
22. Rada C, Williams GT, Nilsen H, Barnes DE, Lindahl T, Neuberger MS. Immunoglobulin isotype switching is inhibited and somatic hypermutation perturbed in UNG-deficient mice. Curr Biol 2002;12:1748–55.
23. Schwede T, Kopp J, Guex N, Peitsch MC. SWISS-MODEL: an automated protein homology-modeling server. Nucleic Acids Res 2003;31:3381–5.
24. Sakurai S, Kitano K, Yamaguchi H, et al. Structural basis for recruitment of human flap endonuclease 1 to PCNA. EMBO J 2005;24:683–93.
25. Hwang KY, Baek K, Kim HY, Cho Y. The crystal structure of flap endonuclease-1 from *Methanococcus jannaschii*. Nat Struct Biol 1998;5:707–13.
26. Schrader CE, Edelmann W, Kucherlapati R, Stavnezer J. Reduced isotype switching in splenic B cells from mice deficient in mismatch repair enzymes. J Exp Med 1999;190:323–30.
27. Hennessy BT, Hanrahan EO, Daly PA. Non-Hodgkin lymphoma: an update. Lancet Oncol 2004;5:341–53.
28. Shipp MA, Ross KN, Tamayo P, et al. Diffuse large B-cell lymphoma outcome prediction by gene-expression profiling and supervised machine learning. Nat Med 2002;8:68–74.
29. Lindahl T. Instability and decay of the primary structure of DNA. Nature 1993;362:709–15.
30. Larsen E, Meza TJ, Kleppa L, Klungland A. Organ and cell specificity of base excision repair mutants in mice. Mutat Res 2007;614:56–68.
31. Xie Y, Yang H, Cunanan C, et al. Deficiencies in mouse Myh and Ogg1 result in tumor predisposition and G to T mutations in codon 12 of the K-ras oncogene in lung tumors. Cancer Res 2004;64:3096–102.
32. Pasqualucci L, Neumeister P, Goossens T, et al. Hypermutation of multiple proto-oncogenes in B-cell diffuse large-cell lymphomas. Nature 2001;412:341–6.
33. Lenburg ME, Sinha A, Faller DV, Denis GV. Tumor-specific and proliferation-specific gene expression typifies murine transgenic B cell lymphomagenesis. J Biol Chem 2007;282:4803–11.
34. Frith CH, Ward JM, Chandra M. The morphology, immunohistochemistry, and incidence of hematopoietic neoplasms in mice and rats. Toxicol Pathol 1993;21:206–18.
35. Schultz-Norton JR, Walt KA, Ziegler YS, et al. The DNA repair protein Flap endonuclease-1 (FEN-1) modulates estrogen-responsive gene expression. Mol Endocrinol 2007;21:1569–80.
36. Nikitin AY, Alcaraz A, Anver MR, et al. Classification of proliferative pulmonary lesions of the mouse: recommendations of the mouse models of human cancers consortium. Cancer Res 2004;64:2307–16.
37. Percy DH, Barthold SW. Pathology of laboratory rodents and rabbits. 2nd ed. Ames (IA): Iowa State University Press; 2001.
38. Zheng L, Dai H, Zhou M, et al. Fen1 mutations result in autoimmunity, chronic inflammation and cancers. Nat Med 2007;13:812–9.
39. Shen M, Zheng T, Lan Q, et al. Polymorphisms in DNA repair genes and risk of non-Hodgkin lymphoma among women in Connecticut. Hum Genet 2006;119:659–68.
40. Zheng L, Dai H, Qiu J, Huang Q, Shen B. Disruption of the FEN-1/PCNA interaction results in DNA replication defects, pulmonary hypoplasia, pancytopenia, and newborn lethality in mice. Mol Cell Biol 2007;27:3176–86.
41. Huggins CF, Chafin DR, Aoyagi S, Henricksen LA, Bambara RA, Hayes JJ. Flap endonuclease 1 efficiently cleaves base excision repair and DNA replication intermediates assembled into nucleosomes. Mol Cell 2002;10:1201–11.
42. Vijayakumar S, Chapados BR, Schmidt KH, Kolodner RD, Tainer JA, Tomkinson AE. The C-terminal domain of yeast PCNA is required for physical and functional interactions with Cdc9 DNA ligase. Nucleic Acids Res 2007;35:1624–37.
43. Wang W, Bambara RA. Human Bloom protein stimulates flap endonuclease 1 activity by resolving DNA secondary structure. J Biol Chem 2005;280:5391–9.
44. Mostoslavsky R, Chua KF, Lombard DB, et al. Genomic instability and aging-like phenotype in the absence of mammalian SIRT6. Cell 2006;124:315–29.
45. Vartanian V, Lowell B, Minko IG, et al. The metabolic syndrome resulting from a knockout of the NEIL1 DNA glycosylase. Proc Natl Acad Sci U S A 2006;103:1864–9.
46. Gerken T, Girard CA, Tung YC, et al. The obesity-associated FTO gene encodes a 2-oxoglutarate-dependent nucleic acid demethylase. Science 2007;318:1469–72.
47. Renehan AG, Tyson M, Egger M, Heller RF, Zwahlen M. Body-mass index and incidence of cancer: a systematic review and meta-analysis of prospective observational studies. Lancet 2008;371:569–78.